

# Reservoir Characteristics and Influencing Factors of the Jurassic Yan'an Formation in the Hao Tan Area of the Ordos Basin

Jiahao Wang<sup>1,2</sup>, Jingyuan Liu<sup>1,2</sup>, Daxi Xu<sup>3</sup> & Yuanshou Zhao<sup>4</sup>

<sup>1</sup> School of Geoscience and Engineering, Xi'an ShiYou University, Xi'an 710065, Shaanxi, China

<sup>2</sup> Shaanxi Provincial Key Laboratory of Oil and Gas Formation and Reservoir Geology, Xi'an 710065, Shaanxi Province, China

<sup>3</sup> 4th Gas Production Plant, Changqing Oilfield Branch, PetroChina, Xi'an 710018, Shaanxi, China

<sup>4</sup> 4th Oil Production Plant, Changqing Oilfield Branch, PetroChina, JingBian 718500, Shaanxi, China

Correspondence: Daxi Xu (1985-), male, Lianyungang, Jiangsu Province, engineer, mainly engaged in oil and gas extraction. E-mail: 250789676@qq.com

Author's Profile: Jiahao Wang (2000-), male, master's degree student, mainly engaged in comprehensive research in petroleum geology. E-mail: wgqwbc1999@163.com

Received: April 22, 2025; Accepted: May 20, 2025; Published: May 22, 2025

## Abstract

To study the reservoir characteristics and main controlling factors of Jurassic Yan'an formation in Hao Tan area of Ordos Basin. The reservoir characteristics and its main controlling factors were revealed by the experimental observations such as rock sheet analysis, high pressure mercury pressure experiment and cathodoluminescence. The Jurassic reservoirs in Hao Tan area are mainly located in Yan 10~Yan 8 section. The results show that the main types are feldspathic sandstone and feldspathic quartz sand with medium to low maturity, and the main types of pores include intergranular pores, intergranular dissolution pores and feldspathic dissolution pores. The physical properties of the reservoir are dominated by mesopore mesoturbidity, with medium throat radius and low drainage pressure. The reservoir has experienced moderate to strong mechanical compaction with various types of cementation dominated by carbonate, siliceous and clay minerals, among which the pore structure of the reservoir has been significantly improved by dissolution. The reservoirs of the Yan'an Formation have certain storage capacity and development potential, especially the Yan 10 and Yan 8 reservoirs have better physical properties, and the sedimentation and diagenesis have affected the inhomogeneity of the reservoirs. It is concluded that the Yan 8 reservoir (72% class II) and the local sweet spot of Yan 10 (class I porosity >16%) have development potential, but different development strategies should be formulated for the high permeability zone of Yan 9. The results of the study can provide a theoretical basis for the exploration and development of the same type of Jurassic tight sandstone reservoirs in the Ordos Basin.

**Keywords:** reservoir characterization, diagenesis, influence factors, Hao Tan, Ordos Basin

## 1. Introduction

Against the backdrop of accelerated energy transition in China, energy security has emerged as a critical national priority [1]. Domestic oil and gas enterprises continue to prioritize "reserve expansion and production enhancement" as their strategic focus. Notably, the Changqing Oilfield achieved a year-on-year increase of 206,000 tons in crude oil production during the first half of 2024, reinforcing its dominant position in China's hydrocarbon production landscape. The Ordos Basin, with over a century of exploration history, maintains pivotal status in China's energy supply system due to its substantial oil and gas resources.

Within the Jurassic Yan'an Formation of the Ordos Basin, particular attention has been drawn to the lower reservoir section characterized by favorable pore architecture, enhanced hydrocarbon mobility, and concentrated oil-bearing strata. These reservoirs exhibit relatively small-scale but high-yield potential [3,4]. The paleogeomorphic lobate river sand reservoirs of the Jurassic system demonstrate distinct features including shallow burial depth, elevated productivity, and compact yet productive characteristics. While reservoir formation involves multiple controlling factors, paleogeomorphological constraints predominantly govern Lower Jurassic reservoirs [5]. Current research indicates that hydrocarbon enrichment in the lower Yan'an Formation correlates closely with pore evolution, where diagenetic processes and cementation types exert significant influences on reservoir petrophysical properties [5].

Nevertheless, comprehensive understanding remains elusive regarding the impacts of pore structure evolution on hydrocarbon migration mechanisms and production capacity, particularly in the Hao Tan area.

Although preliminary oil testing in the Yan 8-Yan 10 formations has yielded promising results, critical knowledge gaps persist in three key aspects: 1) reservoir enrichment mechanisms, 2) pore evolution in tight sandstones, and 3) depositional characteristics with associated heterogeneity [9]. Previous studies have emphasized the fundamental importance of Jurassic reservoir formation conditions and pore structure evolution in hydrocarbon accumulation processes [10]. Systematic investigation of reservoir characteristics and hydrocarbon storage mechanisms in the lower Yan'an Formation bears both theoretical significance for sedimentary basin analysis and practical implications for optimizing exploration efficiency and enhancing residual oil recovery.

This multidisciplinary study employs an integrated analytical approach combining thin-section petrography, high-pressure mercury intrusion porosimetry (MIP), and cathodoluminescence microscopy. The methodology enables: 1) mineralogical characterization and pore-fracture system quantification, 2) determination of key petrophysical parameters (porosity, permeability) governing reservoir storage and flow capacity, and 3) nanoscale pore architecture visualization through scanning electron microscopy (SEM). By correlating petrophysical data with geological constraints, we establish a robust evaluation framework for reservoir quality determinants. These findings provide critical insights for strategic decision-making in hydrocarbon exploration and development optimization.

### 2. Geological Background

The Hao Tan area is located in Dingbian County, Shaanxi Province, in the eastern part of the Hutianshan oil field, with an area of about 616 square kilometers. The area is located at the southern edge of the Ordos Basin, close to the northwest, specifically east of Dingbian area. It is bordered by Ningzhangliang Town of Jingbian County in the east, Zhouwan Town of Wuji County of Yan'an City in the south, Shidonggou Town in the west, and Dupuzhiliang Town in the north. The location of the study area is shown below (Fig. 1)

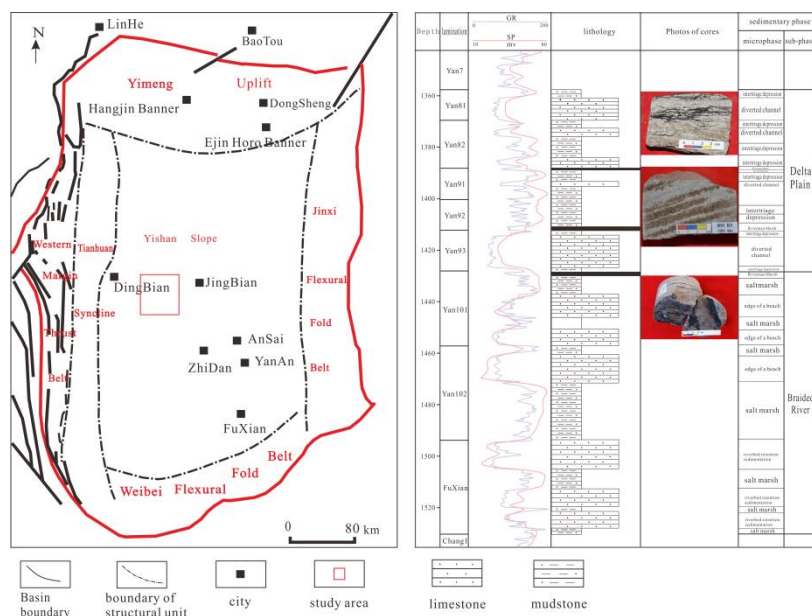


Figure 1. Location of the study area and stratigraphic division and reservoir

The sedimentary characteristics of the area studied by a large number of predecessors indicate that at the end of the Triassic, the Ordos Basin was uplifted by the Indo-Chinese movement, and the strata of the Extension Formation were widely denuded to form eroded valleys widely developed in the pre-Jurassic paleogeomorphic features. On the background of this paleomorphology, the early (Yan10+Fuxian) fluvial sedimentary filling and the middle and late (Yan9-Yan4+5) river and lake phases developed constituted the first Jurassic depositional cycle, i.e., fluvial phase-deltaic phase-lake erosion and deposition of the shallow lake phase [24].

One of the main stratigraphic layers for oil and gas exploration in Hao Tan area is Jurassic, and the unconformity at the bottom of thick sandstone of Zhiluo Formation and the unconformity between the Jurassic and Triassic are the regional marker layers; followed by Yan 6, Yan 7, Yan 8, Yan 9, and Yan 10 top coal seams as the auxiliary

marker layers; the regional marker layers and the top coal marker layers have stable distribution and are highly comparable. In the next step, the main Jurassic seam in the study area, Yan 8, is subdivided into Yan 81 and Yan 82, Yan 9 is subdivided into Yan 91, Yan 92, and Yan 93, and Yan 10 is subdivided into Yan 101 and Yan 102, with a total of 7 small seams.

### 3. Reservoir Characteristic

#### 3.1 Lithological Feature

Analysis of the Yan'an Formation in the study area shows that it is mainly composed of feldspathic sandstone, feldspathic quartz sandstone and clastic feldspathic sandstone. These rock types are of medium-low maturity and have a high quartz content. The clastic composition is dominated by metamorphic and igneous rocks, while other clastic compositions mainly consist of mica. The fillings are low and are dominated by kaolinite, followed by siliceous material, with small amounts of calcite and iron calcite (Figure 2).

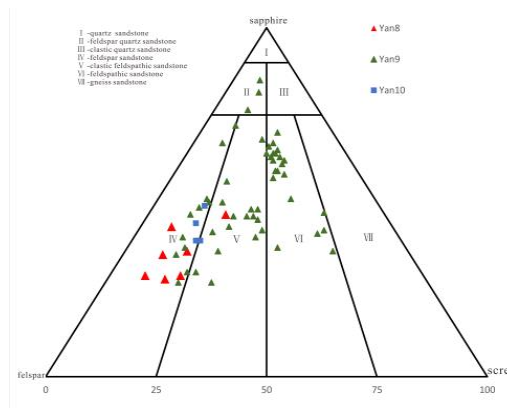


Figure 2. Typology of Yan8-Yan10 reservoir sandstones in the study area Petrographic analysis of core samples from study area wells, employing plane-polarized light microscopy and cathodoluminescence (CL) imaging, revealed distinct mineralogical characteristics.

Feldspar grains exhibit well-defined cleavage planes under plane-polarized light with grayish-white coloration, while CL responses (orange-red and brown emissions) indicate dual provenance from both primary basin sources and altered igneous materials (Fig. 3a,c). In contrast, quartz grains show similar optical properties under plane-polarized light but lack cleavage features, predominantly displaying blue CL emissions or CL-inert behavior. Lithic fragments and interstitial matrix components generally demonstrate CL-inactive characteristics, with sporadic blue, orange-red, or violet CL speckles corresponding to microcrystalline quartz, feldspar, or calcite cementation (Fig. 3b,d). These CL signatures provide critical constraints on diagenetic histories and sediment provenance within the reservoir system.

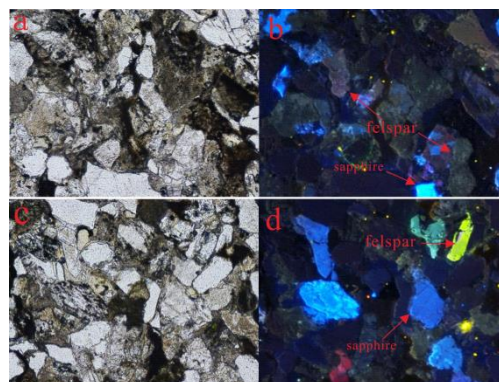


Figure 3. Photographs of rocky single polarization and cathodoluminescence  
 a) Lithic arkose from Well A123, Yan8 Formation (1331.05 m depth), 10× plane-polarized light  
 b) Lithic arkose from Well A123, Yan8 Formation (1331.05 m depth), 10× cathodoluminescence  
 c) Lithic arkose from Well H175, Yan9 Formation (1309.25 m depth), 10× plane-polarized light

d) Lithic arkose from Well H175, Yan9 Formation (1309.25 m depth), 10× cathodoluminescence

3.2 Textural Characteristics

Integrated analysis of measured pore architecture and petrophysical properties, combined with collated datasets, reveals distinct porosity-permeability characteristics within the principal target intervals. Statistical evaluation demonstrates favorable reservoir quality across the study horizons, with porosity ranging from 14.8% to 17.5% and permeability spanning 10.2–103.5 mD. Enhanced permeability is particularly evident in the Yan8<sup>2</sup>–Yan10 intervals, while porosity exhibits relatively uniform spatial distribution. A robust exponential correlation ( $R^2 > 0.80$ ) is observed between porosity and permeability, indicative of pore-throat connectivity dominated by intergranular and dissolution-related pore systems (Fig. 4).

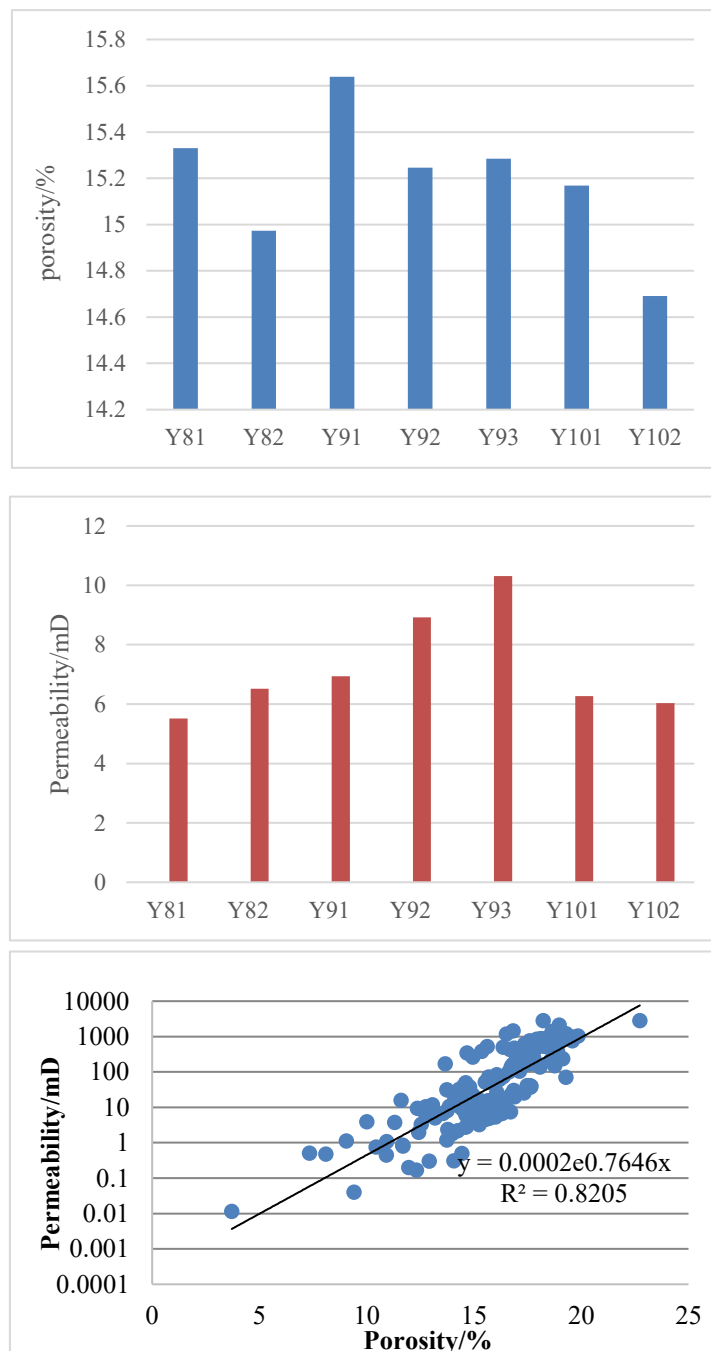


Figure 4. Plot of permeability-porosity relationship and histogram of porosity-permeability frequencies

3.3 Textural Characteristics

Grain-size probability cumulative analysis reveals distinct textural attributes within the study area. The sedimentary samples exhibit coarse-skewed distributions with a mean grain size of  $1.09\phi$  (~0.464 mm) and standard deviation of  $0.53\phi$ , indicative of broad particle size dispersion and moderate sorting efficiency. Grain-size distributions display a leptokurtic pattern dominated by medium-to-coarse sand fractions (60-75% content), with limited fine-grained components (<5% suspended load). Bivariate probability plots demonstrate bimodal transport dynamics, characterized by: Saltation populations with slope angles of  $55-65^\circ$  Fine truncation points at  $2.5-3.5\phi$

C-M diagram analysis (C = 0.51 mm, M = 0.29 mm) confirms graded suspension deposition under tractive current regimes, reflecting hybrid hydrodynamic conditions with alternating energetic and quiescent phases. Textural maturity indices suggest moderately advanced diagenetic modifications, evidenced by: Subangular-to-subrounded grain morphologies Preferred grain orientation (80% long-axis alignment within  $\pm 15^\circ$ ) Stable interstitial packing geometries Notably, the Yan10 sandstone exhibits coarser texture (35-45% medium sand, 15-20% coarse sand) compared to other intervals, suggesting proximal source input during high-energy depositional events (Fig. 4; Table 1).

Table 1. Statistical table of particle size distribution and parameters in the study area

Layer	Grain size distribution (%)					Middle sand and above (%)	Fine sand and below (%)	Particle size parameters		Number of samples (pieces)
	Coarse sand	Medium sand	Fine sand	Powdered sand	Clay			C value (mm)	M value (mm)	
Extended 8	5.4	31.3	58.8	4.3	0.2	36.7	63.3	0.44	0.20	11
Extension 9	10.4	36.2	50.0	2.5	0.9	46.5	53.5	0.56	0.27	35
Extended 10	22.0	33.4	40.4	1.2	3.0	55.4	44.6	0.70	0.30	20

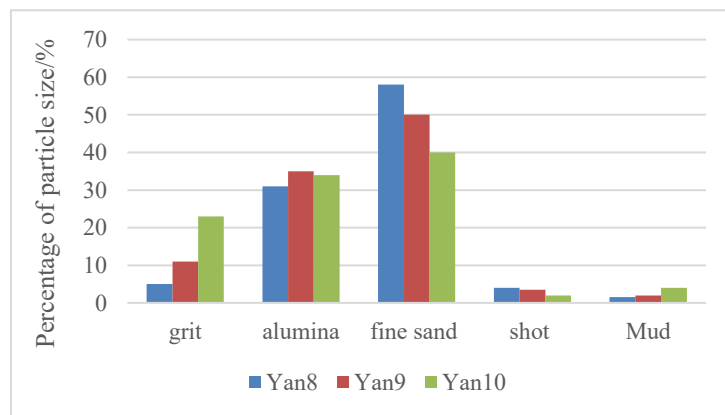


Figure 4. Statistical histogram of grain size analysis of sandstone in the main layer of Yan'an Formation

3.4 Reservoir Space Characteristics

The target intervals exhibit dual-porosity systems dominated by intergranular pores (62-78% volumetric contribution), with subordinate feldspar dissolution pores (15-22%) and minor intragranular microporosity (<5%). Quantitative analysis demonstrates stratigraphically controlled pore geometry variations:

Yan8 Formation: Average porosity of 12.3% with 65-70% intergranular pore dominance

Yan9 Formation: Enhanced porosity (14.6%) featuring 55-60% intergranular pores and 25-30% dissolution-enhanced voids

Yan10 Formation: Reduced porosity (11.2%) dominated by compacted intergranular pores (75-82%)

Spatial correlation analysis reveals intergranular pore connectivity ( $R^2=0.83$ ) as the primary control on reservoir quality, while dissolution porosity shows weaker correlation ( $R^2=0.41$ ) due to localized diagenetic overprinting. These pore architectures reflect competing diagenetic processes: Porosity-enhancing mechanisms:

Selective feldspar dissolution along cleavage planes Early chlorite rim cementation preserving pore throats  
 Porosity-reducing mechanisms: Quartz overgrowth occlusion (15-20% pore volume reduction) Mechanical compaction-induced pore distortion (Fig. 5) The Yan9 Formation's superior porosity-permeability synergy suggests optimal balance between primary porosity preservation and secondary dissolution enhancement, providing critical implications for sweet spot identification.

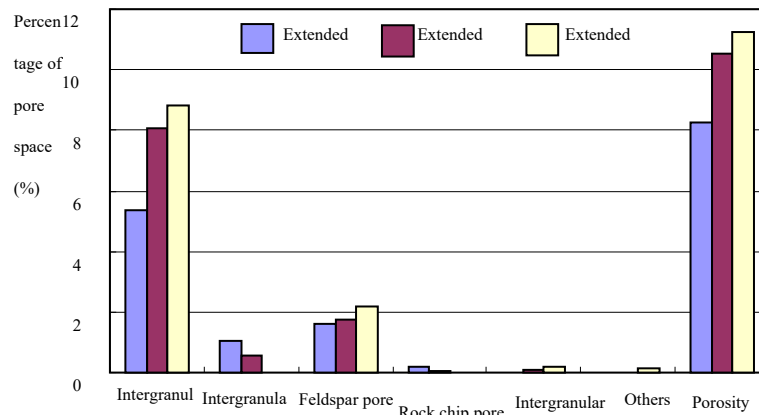


Figure 5. Table of pore occupancy in the study area

Mercury injection capillary pressure (MICP) analysis delineates distinct reservoir quality tiers across target intervals (Table 2). The Yan8 Formation exhibits moderate petrophysical properties ( $\Phi=15.4\%$ ,  $K=98.9$  mD) with homogeneous pore-throat distribution (sorting coefficient=2.1) and favorable mercury withdrawal efficiency (31.4%), indicating well-connected pore networks suitable for stable production deployment. In contrast, the Yan9 Formation demonstrates extreme permeability contrasts ( $K=12.7-1170.6$  mD), where high-permeability zones (e.g., Well H37: 1170.6 mD) suggest fracture networks or preferential flow channels. However, anomalously low withdrawal efficiency (8.89% in H37) reveals localized pore isolation, likely caused by: Fracture-matrix decoupling during mercury extrusion Authigenic kaolinite plugging of connecting throats This heterogeneity necessitates advanced saturation monitoring and conformance control strategies during late-stage development. The Yan10 Formation presents a porosity-permeability paradox ( $\Phi=16.45\%$ ,  $K=7.39$  mD) with suboptimal withdrawal efficiency (21.9%), reflecting poor pore connectivity despite abundant void space. Pore-throat size distribution analysis identifies dual constraints: 68% of pores  $<1 \mu\text{m}$  diameter Throat radius mode=0.3  $\mu\text{m}$  Development recommendations prioritize: Yan9 sweet spots: Pilot production focusing on high-permeability corridors ( $K>500$  mD) Yan8: Base-load production with waterflood pressure maintenance Yan10: Economically constrained stimulation through hybrid acid-proppant fracturing This tiered development strategy optimizes resource recovery while mitigating heterogeneity-related risks through: Real-time production logging in Yan9 Nanoscale-proppant applications in Yan10 Intelligent well completions for zonal isolation

Table 2. Experimental Data Sheet for Mercury Piezoelectricity

Well No.	Depth (m)	Layer	Porosity (%)	Permeability (mD)	Discharge pressure (Mpa)	Median pressure (Mpa)	Median radius ( $\mu\text{m}$ )	Maximum SHg (%)	De-mercurizing efficiency (%)	Sorting coefficient	Variation Coefficient
A119	1260.93	Extended 8	16.2	16.8	0.13	2.3	0.32	79.05	33.41	2.55	0.24
A123	1337.6	Extension 8	21.6	153.6	0.5	5.57	0.13	88.37	32.21	2.22	0.17
A238	1260.8	Extension 8	18.9	225.3	0.33	3.95	0.19	86.58	32.32	2.25	0.18
X15	1291.8	Extension 8	4.9	0.06	0.4	5.43	0.14	87.75	27.66	2.39	0.18
Average			15.4	98.9	0.34	4.31	0.19	85.44	31.4	2.35	0.19
H37	1298.2	Extension 9	18.8	1170.6	0.01			99.53	8.89	2.74	
H175	1309.25	Extended 9	12.6	10.3	0.51	5.06	0.15	87.55	29.82	2.23	0.17

H83	1277.4	Extended 9	18.3	228.5	0.4	5.58	0.13	86.11	32.51	2.33	0.18
S269	1301.1	Extension 9	9.8	0.4	0.4	4.51	0.16	87.66	30.9	2.32	0.18
X22	1303.7	Extension 9	15.7	24	0.225	4.321	0.17	65.6	44.34	2.47	0.22
X43	1344.9	Extension 9	17.4	13.4	0.51	4.54	0.16	85.36	28.06	2.28	0.17
Average			15.4	241.2	0.34	4.8	0.15	85.3	29.09	2.4	0.18
A16	1929.55	Extension10	15.8	1.8	0.408	2.919	0.25	77.4	23.1	2.4	0.21
A16	1941.6	Extension10	17.1	13	0.168	1.464	0.5	80.7	20.7	2.84	0.27
Average			16.45	7.39	0.29	2.19	0.375	79.05	21.9	2.62	0.245

#### 4. Reservoir Controlling Factors

Following the petroleum industry standard SY/T 6285-2011 ("Evaluation Methods for Oil and Gas Reservoirs"), the study area reservoirs are classified into Type I–III based on integrated sedimentological, diagenetic, and petrophysical criteria.

##### 4.1 Depositional Controls on Reservoir Quality

The depositional environment exerts a profound influence on the initial architecture of the reservoir by regulating the development of primary porosity through the action of hydrodynamic energy regimes. The properties of a clastic reservoir, such as its texture, composition, bed thickness, and subsequent diagenetic potential, are fundamentally constrained by depositional processes. The following key mechanistic relationships have been identified:

**Hydrodynamic Energy Gradients:** In the context of high-energy settings, such as channel thalwegs, the formation of well-sorted, coarse-grained sands with primary porosity exceeding 25% is promoted.

In low-energy environments, such as floodplains, the accumulation of fine-grained, clay-rich sediments is observed, characterized by an initial porosity of less than 15%. **Facies Belt Architecture:** Braided river systems are characterized by the formation of vertically stacked, homogeneous sand bodies, with a thickness ranging from two to five meters. Meandering river deposits demonstrate lateral heterogeneity, manifesting as mud drapes and inclined heterolithic stratification. **Sediment Sorting Dynamics:** In the context of high-energy regimes, the truncation of fine fractions has been demonstrated to have a significant impact on enhancing pore-throat connectivity.

The presence of matrix-rich sediments in abandoned channels has been observed to result in the formation of permeability baffles. Thin-section analysis (Fig. 6) reveals depositionally induced pore-filling patterns, where fluvial channel sands retain 60–75% primary intergranular porosity, while overbank facies show >40% porosity reduction due to infiltrated clays. The observations presented herein corroborate the hypothesis that depositional environment is the primary factor influencing reservoir heterogeneity.

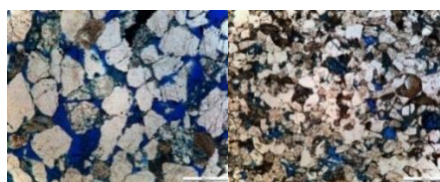


Figure 6. Thin section observation of well H833. a) Well H83, Yan<sup>9</sup>1 Formation (1277.40 m depth), 5× plane-polarized light; b) Well H83, Yan<sup>10</sup>2 Formation (1345.66 m depth), 5× plane-polarized light

##### 4.2 Diagenetic Controls on Reservoir Development

Diagenesis critically shapes tight sandstone reservoir architecture through compaction, cementation, and dissolution-alteration processes (Fig. 7). These modifications, governed by burial history and fluid-rock interactions, ultimately determine reservoir quality heterogeneity.

###### 4.2.1 Compaction

Mechanical compaction dominates porosity destruction (14.8% average loss) in Yan'an Formation reservoirs. Quantitative analysis using Beard & Weyl's formula:

$$\Phi_0 = 20.91 + 22.9/S_0 \quad (1)$$

(where  $S_0 = (\Phi_{50} - \Phi_{16})/4 + (\Phi_{95} - \Phi_5)/6.6$ ) reveals original porosity averaging 30.27% for Yan8-Yan10 intervals. Progressive vertical compaction intensity is evidenced by: Grain contact evolution: Concave-convex → Point contacts from Yan10 to Yan8 (Figs. 7a,b) Plastic component distortion: 15-20% ductile lithics compressed into pseudomatrix Rigid grain rearrangement: 60-70% quartz/feldspar grains show preferred orientation

Early chlorite coatings (1-6 μm thick) and calcite cementation preserved 12-18% porosity by resisting grain rearrangement.

4.2.2 Cementation

Carbonate Cementation Three-phase calcite cementation history is identified: Micritic Calcite: Matrix-support texture in fine sands ( $\phi < 0.1$  mm), reducing porosity to <8% Sparry Calcite: Poikilotopic cement filling dissolution-enhanced pores (Figs. 7c-e) Ferroan Calcite: Purple-stained pore-filling cement (Fig. 7f) with limited distribution

Dolomite/ankerite preferentially replaces calcite along dissolution surfaces (Figs. 7g), while siderite preserves relict feldspar outlines through pseudomorphic replacement.

Silica Cementation

Quartz cementation modes include: Overgrowths: 2-5 μm thick euhedral rims reducing throat radii by 49% (Table 4) Monocrystalline Quartz: <10 μm crystals forming pore-lining "quartz lawns" (Fig. 7h)

Cathodoluminescence reveals growth zoning with fluid inclusions (Fig. 7i), indicating episodic SiO<sub>2</sub> supply from feldspar dissolution. Chlorite coatings effectively inhibited quartz overgrowth, preserving 15-20% intergranular porosity.

Clay Mineral Cementation

Clay diagenesis follows the paragenetic sequence: Chlorite rims (5-12 μm) → 2. Kaolinite booklets → 3. Illite fibers Key impacts: Chlorite: Reduces permeability by 1-2 orders but preserves microporosity Kaolinite: Vermicular aggregates create 0.1-1 μm tortuous throats (Hg efficiency 21.9%) Illite: Hair-like bridging decreases pore connectivity index by 0.3-0.5 (Fig. 7j,k)

4.2.3 Dissolution & Replacement

The process of metastable component dissolution, characterized by the presence of 18–23% feldspar and 5–8% lithics, resulted in the formation of secondary porosity through a series of complex geological processes.

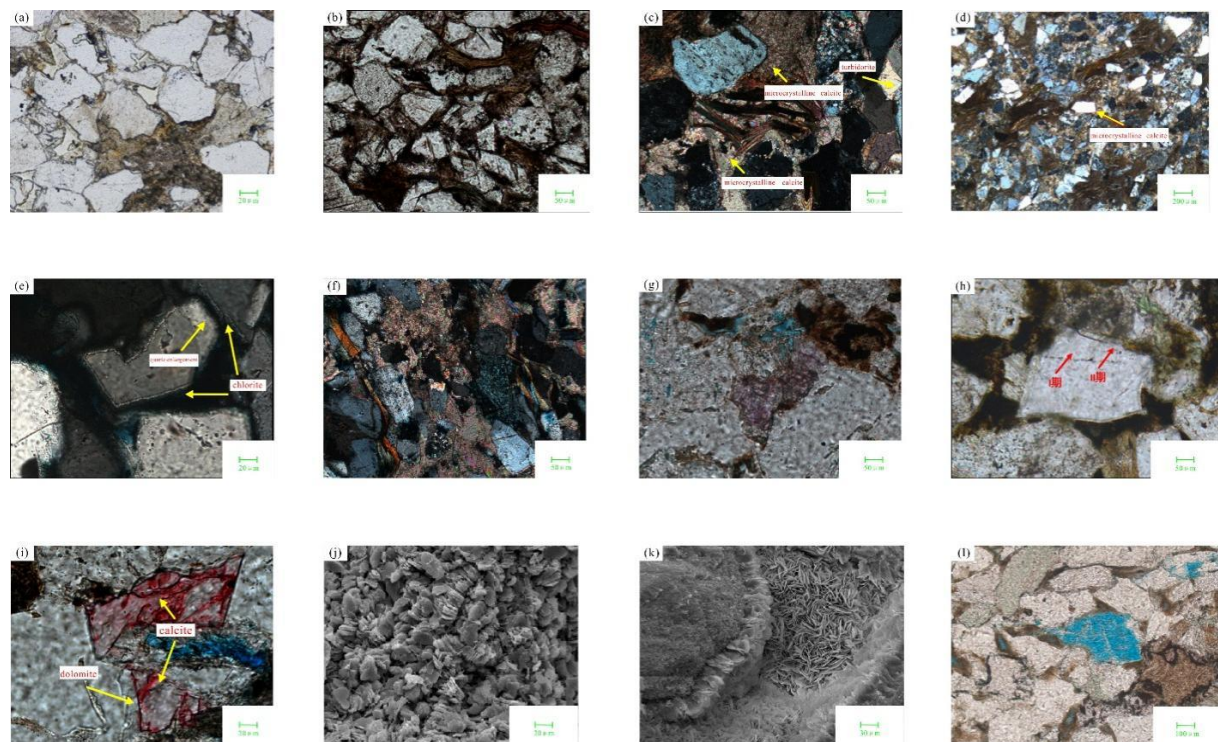


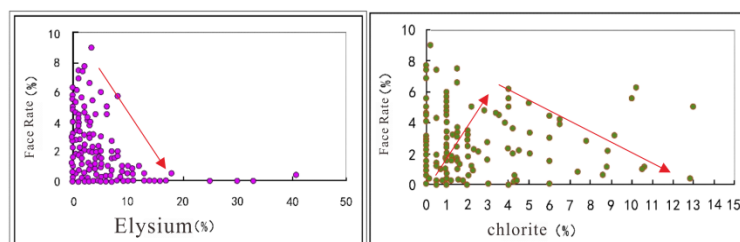
Figure 7. Photographs of thin-section observations of diagenesis in the study area

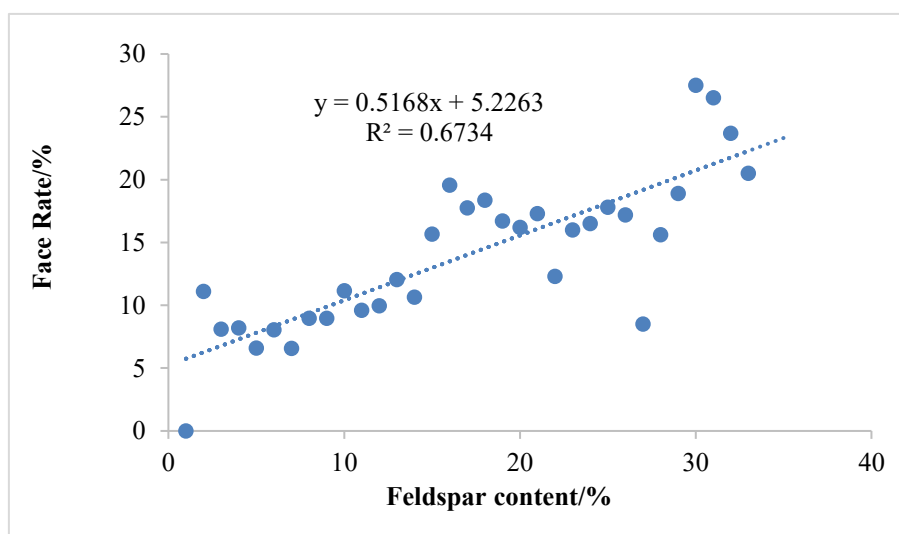
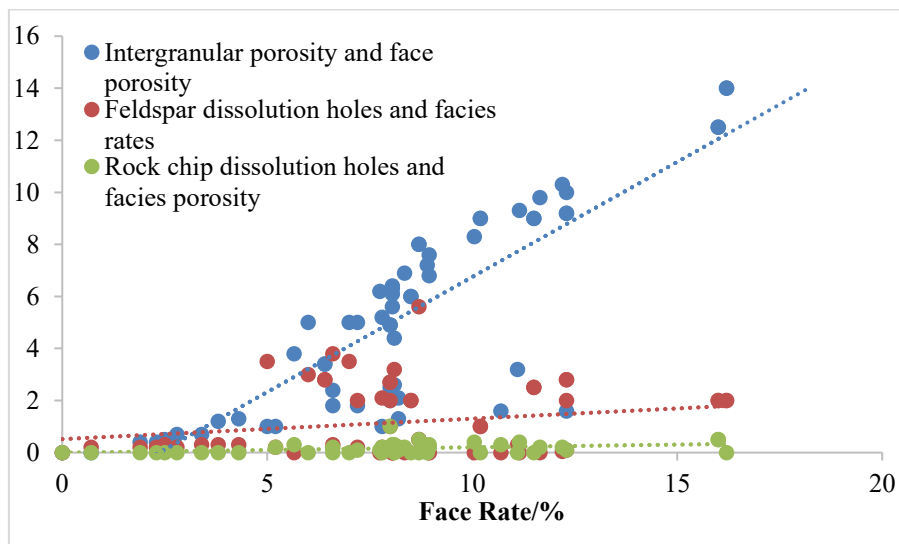
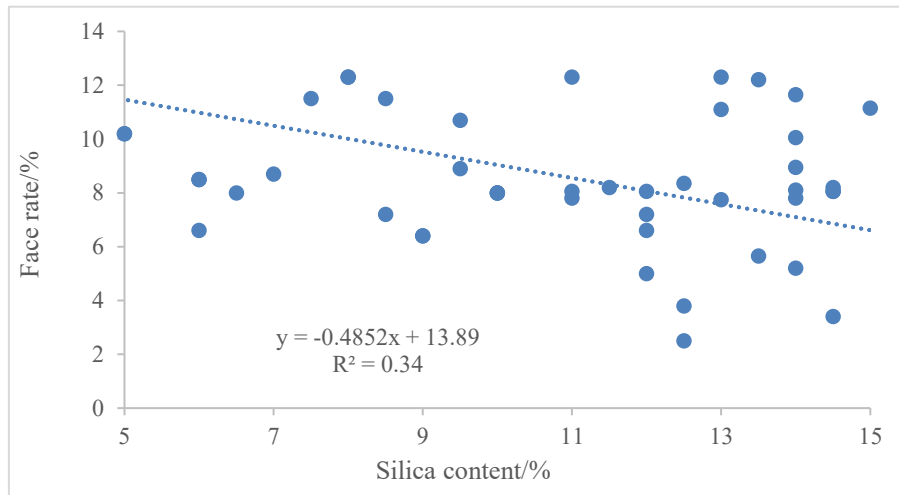
Feldspar Albitization: The generation of dissolution pores measuring between 5 and 20 micrometers has been observed in a range of Na-rich fluids. The process of carbonate replacement is defined as follows: The presence of sparry calcite is indicated in the figure, with micritic precursors being replaced (Fig. 7i). The transformation of clay minerals is a subject of interest in the field of geology. The process of illitization of smectite consumes 15–20% of the porewater  $K^+$ . The presence of authigenic mineral assemblages indicates the existence of two distinct fluid regimes: The initial stage of the process is marked by an acidic environment, with a pH range of 4 to 5, as indicated by the presence of organic carbon dioxide. This stage is characterized by the dissolution of feldspar, a process driven by the aforementioned acidic conditions. The late alkaline stage, characterized by a pH range of 7–8, is conducive to the promotion of illite growth through the process of K-feldspar alteration.

a Particle point-line contact. H83 borehole, extension 9,1277.40m, 10x single polarized light; b Mica deformed by extrusion. H37 borehole, extension 8,1295.50m, 10x single polarized light; c X44 borehole, extension 8,1275.15m, 10x orthorhombic light; d H83 borehole, extension 9,1276.60m, 10x orthorhombic light; e Quartz secondary plus large edges and clastic grains H175 borehole, extension 10,1309.25m, 50x single polarized light; f H37 drill hole, extend 8,1295.50m, 10x orthorhombic light leucite calcite; g A238 drill hole, extend 8,1260.80m, 10x single polarized light iron calcite; h Two phases of quartz secondary enlargement. h H83 hole, 9,1276.60m extension, 10x single polarized light; i A123 hole, 8, 1331.05m extension, 10x single polarized light; j Wormy kaolinite, H83 hole, 9, 1276.60m, SEM; k Autochlorite thin film, H83 hole, Extension 9, 1277.40m, SEM; i Intragranular lysoconite in feldspar grains, dissolution occurs along feldspar solution, H83 hole, Extension 9, 1276.60m, 10x stained thin section.

#### 4.2.4 Diagenetic Process Interrelationships

Ilmenite formation occurs through two predominant mechanisms: clastic deposition and authigenesis. Of these, detrital deposition leads to the filling of pores and throats, complicating the otherwise simple pore-throat structure and thus reducing the physical properties of the reservoir (Fig. 8a). During the initial stages of early diagenesis, chlorite is typically present as a thin film in the pore lining. This presence inhibits contemporaneous and slightly later quartz growth and slows the extent of compaction. However, as chlorite growth progresses, it gradually fills the pore space, resulting in the occlusion of the throat and a subsequent reduction in the reservoir's physical properties. As demonstrated in Figure 8b, experimental data reveal a substantial decrease in facies porosity when chlorite content exceeds 4%. The occurrence of siliceous cementation further plugs the pore space by increasing the filling effect of authigenic quartz minerals, and the coarsening of the rock grain size leads to a decrease in the physical properties of the reservoir. Moderate quartz cementation in the early stages of diagenesis has been shown to impede the compaction process (Fig. 8c). When chlorite membranes are high, it has been demonstrated to inhibit the formation of siliciclastic cementation. Conversely, in late diagenesis, sandstones with more mature chlorite development are often filled with late siliciclastic and iron calcite. Conversely, sandstones that do not exhibit chlorite development demonstrate reduced levels of iron calcite and silica. The dissolution process has been shown to enhance reservoir porosity and permeability. The extent of this effect is influenced by a variety of factors, including the size and maturity of clastic particles, the content of soluble components, the production of organic acids, and the interrelationship between compaction and cementation. The primary dissolution process occurs during the late early to early early diagenesis stage, a period in which the dissolution of feldspars, rock fragments, and other aluminosilicate minerals is primarily driven by the presence of organic acids. The study demonstrates that the dissolution porosity of feldspar enhances the reservoir properties within the study horizon in the Hao Tan area (Fig. 8d). Given that the predominant lithology in the study area consists of feldspathic sandstone and clastic feldspathic sandstone, the relationship between feldspar content and porosity is statistically calculated. The calculation results demonstrate a strong positive correlation between feldspar content and porosity (Fig. 8e). The calculation of the average grain size and porosity in the study area demonstrates a strong positive correlation between these parameters (Fig. 8f). This finding suggests a potential relationship between diagenesis and alterations in rock porosity, which may consequently impact reservoir performance. Variations in particle size have been shown to influence the physical properties of the reservoir.





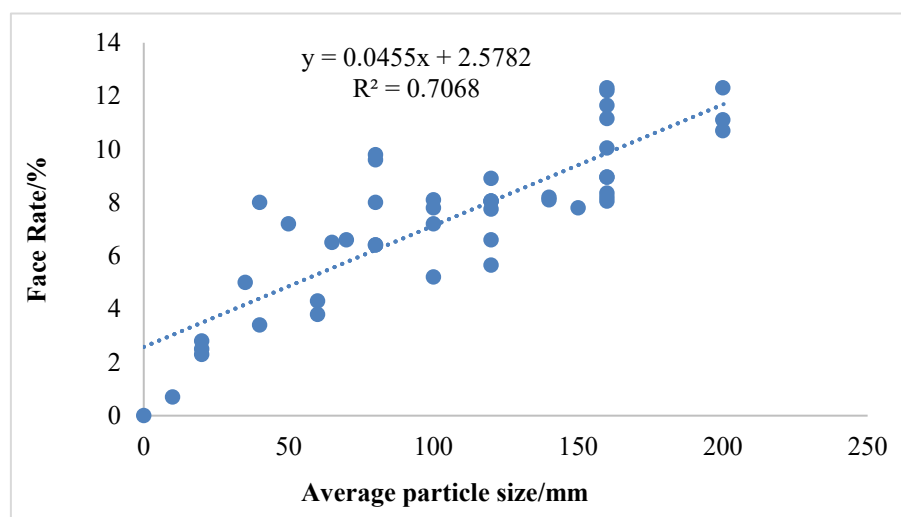


Figure 8. Diagram of diagenetic relationships. A. Plot of illite content versus face porosity at the study horizon; b Plot of chlorite content versus face porosity at the study horizon; c. Plot of siliceous content versus face porosity at the study horizon; d. Plot of type of sedimentation versus porosity; e. Plot of feldspar content versus porosity; f. Plot of mean grain size versus porosity.

## 5. Diagenetic sequence

The sequence of diagenesis in the Hao Tan area was mapped by the diagenesis and reservoir physical characteristics in the study area, combined with the standard for the division of diagenetic stages (SY/T5477-92, 2003) (Fig. 9). And the following diagenetic stage markers are delineated.

The initial diagenetic stage is characterized by the predominance of transformation processes involving mixed layer clay minerals. In the initial phase of burial, montmorillonite minerals were precipitated with pore water, gradually transforming into a mixture of Yi and montmorillonite clays (>50% montmorillonite layer) with increasing temperature (60–80°C) and enrichment of  $K^+$  and  $Al^{3+}$  ions in the pore water. This process occurred in a  $Mg^{2+}$ -rich,  $Fe^{2+}$ -rich environment, resulting in the formation of montmorillonitic clays. Thin section identification indicates that the proportion of montmorillonite layer in the Yimun mixed layer of the Yan 10 level is approximately 35% to 45%, reflecting medium diagenetic strength, and the transformation of clay minerals has not been fully completed.

In the second Intermediate diagenetic stage: The coexistence of Fe-containing carbonate cementation and dissolution has been observed to occur in response to variations in burial depth and temperature. At depths of approximately 80 to 100 degrees Celsius, an increase in temperature leads to the formation of Fe-calcite cement, a mineral composed of  $Fe^{2+}$  and  $CO_3^-$  ions, within the pore water. This cementation process takes place in the intergranular pores of sandstone formations, specifically at the Yan9 level, and results in the formation of patchy or ring-shaped Fe-calcite deposits. Concurrently, the decarboxylation of organic matter precipitates the release of acidic fluids, resulting in the dissolution of feldspars, clasts, and early calcite colloidion, concurrent with the formation of honeycomb dissolution pores. The proportion of dissolution pores in the Yan 8 layer position ranges from 12% to 18%, and the predominant pore combination is residual intergranular pores, accounting for 40% to 50%, and feldspar dissolution pores, accounting for 25% to 35%. The contact relationship of particles is predominantly characterized by point-line contact, exhibiting the characteristics of early linear contact, which are retained in a local manner.

The third phase is the late orogenic stage, which is characterized by secondary quartz enlargement and pore fixation.

The continuous increase in temperature (greater than 120°C) has been shown to promote the massive growth of authigenic quartz. The secondary quartz enlargement generally reaches grade II, which is characterized by continuous thickening of the grain edge (2–5  $\mu m$ ). Localized grade III enlargement has been observed in highly mature sandstones, where grains are in contact mosaic and the throat width is less than 1  $\mu m$ . The occurrence of quartz enlargement in the extended 8-layer position has been observed to result in a rate of throat blockage that falls within the range of 15% to 20%. This phenomenon is accompanied by a subsequent loss of primary pores. However, the preservation of early dissolution pores has been noted, a phenomenon that can be attributed to the

presence of siliceous protection. Presently, sandstone grains are predominantly in point contact, clay mineral transformation is complete (with a montmorillonite layer comprising less than 15% of the Yi/Mongolian mixed layer), and diagenesis exhibits signs of stagnation.

The intensity of diagenesis underwent a transition from strong to weak during the transition from Yan 10 to Yan 8. The Yan 10 phase is distinguished by the occurrence of iron calcite cementation, quartz weak enlargement (Class I), and granular concave-convex contact. The Yan 9 phase is marked by the intensification of dissolution and substantial pore modification. The Yan 8 phase is characterized by widespread secondary enlargement of quartz, accompanied by enhanced preservation of dissolution pore space. The diagenetic sequence is influenced by various factors, including burial history, thermal history, and fluid activity. These factors contribute to the formation of the reservoir pattern, which is characterized by high porosity in "Yan9," medium porosity in "Yan8," and low porosity in "Yan10." In summary, the study demonstrates that the diagenetic sequence is comprised of the following stages: compaction, dissolution, chlorite film/feldspar enlargement, quartz enlargement, calcite cementation, dissolution, kaolinite, calcite cementation, and oil and gas filling. During the Jurassic period, two minor uplifts of the regional stratigraphy occurred, and the stratigraphic slope also exerted an influence on diagenesis as well as hydrocarbon formation. The studied stratigraphy is primarily in the middle-late diagenetic stage A, with occasional instances reaching the middle-late diagenetic stage B. The reservoirs were in the initial phase of oil and gas injection. The reservoirs exhibited superior physical properties during the initial phase of oil and gas injection, demonstrating increased density prior to the large-scale injection. This phenomenon subsequently impacts the physical characteristics of the reservoir in the subsequent stages.

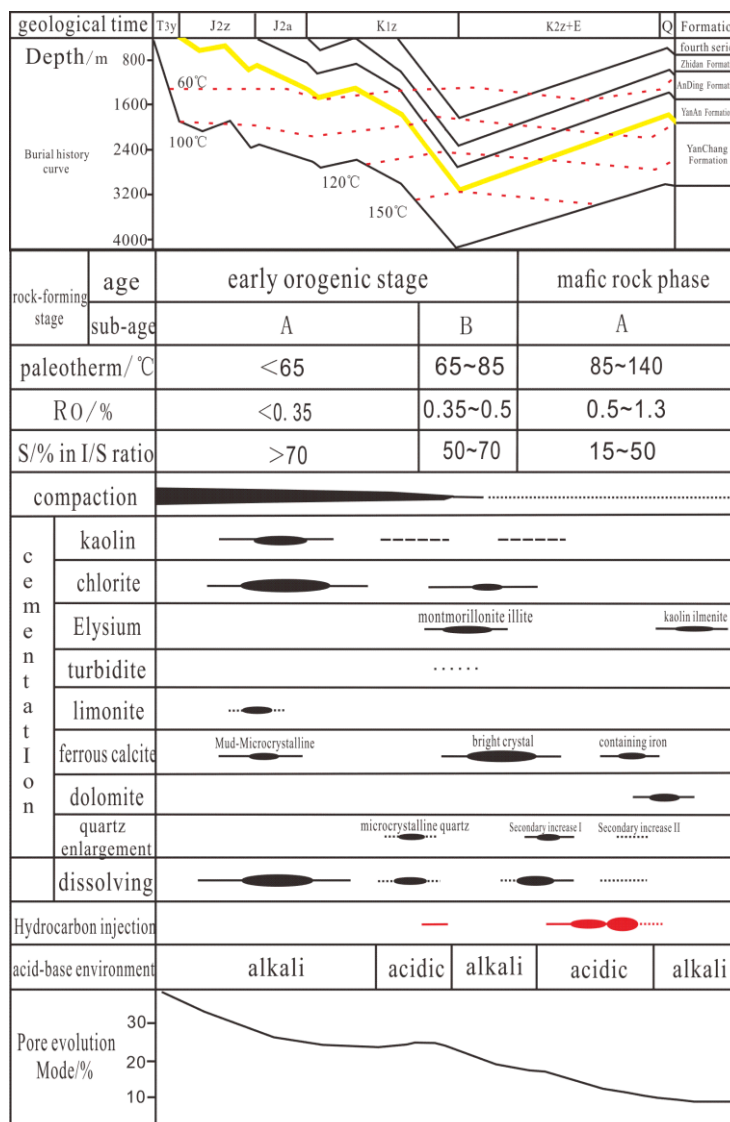


Figure 9. Sequence diagram of diagenetic evolution

### 6. A Prognosis of Profit-Generating Segments

The present study is an in-depth analysis of the regional diagenetic evolution process. This analysis is divided into two phases: the initial phase and the subsequent phase. The primary objective of this study is to predict favorable reservoirs in the Hao Tan area. The prediction is based on the type of reservoir sedimentary phases, effective sandstone thickness, physical properties, casting body flakes, and pore structure classification results. Furthermore, the classification criteria for Mesozoic reservoirs in the basin, as formulated by the Changqing Oilfield Research Institute (see Table 3), were utilized as a reference to evaluate the classification of each layer under study. The Jurassic reservoirs in the Hao Tan area are predominantly Class II reservoirs (58%-72%), which are extensively distributed in the areas of Yan 102, Yan 92-93, and Yan 81-82. These reservoirs exhibit porosities ranging from 12.6-18.3% and permeability values ranging from 10.3-228.5 mD. Additionally, they possess medium storage and permeability capacity. Class I reservoirs, which account for 12-18% of the total, are characterized by their isolation and enrichment at the river confluence. A notable example of this is Yan 101 and Yan 91 local. These reservoirs possess a porosity range of 16.2-21.6% and exhibit permeability levels of up to 225.3mD, as evidenced by the A238 well. This region is recognized as a high-quality desert area. Class III reservoirs, comprising 16-30% of the total, are predominantly found in the river flanks and in areas with weak depositional characteristics. As indicated by the side margins of Yan 102 and the front edge of Yan 81, the porosity is less than 10%, the permeability is less than 1mD, and the permeability is less than 1mD. The permeability of these reservoirs is typically less than 10%, with a median value of 1mD. The transformation of these reservoirs is necessitated by the strong cementation-compaction effect that governs their behavior. In accordance with the principles underlying reservoir selection, it is imperative to enhance the delineation of Class I and Class II reservoirs and to institute corresponding development countermeasures in subsequent stages.

Table 3. Criteria table for classification of reservoirs in the Ordos Basin (according to Changqing Research Institute)

Classification parameters	Reservoir classification		
	I	II	III
Sandstone thickness (m)	>12.0	10.0—8.0	8.0—5.0
Porosity (%)	>15.0	15.0—12.0	12.0—10.0
Permeability (mD)	>10.0	10.0—5.0	5.0—1.0
Filler (%)	<11.0	11.0-12.0	12.0-14.0
Face ratio (%)	>5.0	5.0—3.0	3.0—2.0
Average pore size (μm)	>40	40.0—30.0	30.0—22.0
Maximum throat radius (μm)	>1.5	1.5—1.0	1.0—0.7
Throat sorting coefficient(Sp)	>2.0	2.0—1.5	1.8—1.5
Discharge pressure (Mpa)	<0.5	0.5—1.0	1.0-1.5
Type of pore structure	Large and medium pore size Medium throat type	Large and medium pore size Medium throat type	Medium pore size Fine throat type
Overall evaluation	Good	Better	Medium Fair

### 7. Conclusion

(1)The reservoirs in the Yan'an 8-Yan'an 10 area are primarily composed of feldspathic sandstone and feldspathic quartz sandstone. These reservoirs exhibit a moderate degree of immaturity in their rock composition, with the presence of intergranular and intergranular soluble pores, among other types. The physical characteristics of Yan'an 8 reservoir are predominantly characterized by medium-sized pores and medium seepage. The physical properties of the reservoirs are dominated by medium pores and medium seepage; the Yan 8 reservoir is dominated by Class II, the Yan 9 reservoir is dominated by Class II and Class III, and the Yan 10 reservoir is dominated by Class I and Class II. This indicates that the reservoirs of the Yan'an Formation have a certain storage capacity.

(2) The reservoirs in the study area have experienced moderate to strong mechanical compaction, with various types of cement, mainly carbonate cement, siliceous and clay mineral cement. The grain size distribution of the reservoir is characterized by a coarse texture, the sortability is moderately preferred, and the overall structural maturity is moderately preferred. The joint effect of these characteristics on the seepage capacity and oil storage characteristics of the reservoir is a subject of ongoing research. A series of high-pressure mercury pressure experiments were conducted to obtain key physical parameters, including reservoir porosity and permeability. These experiments yielded insights into the reservoir's seepage capacity and storage performance. The initial

porosity of the reservoir is determined by sedimentation, and diagenesis further enhances its inhomogeneity, as evidenced by significant disparities in pore structure and permeability.

(3) The reservoirs within the study area possess specific storage capacity and development potential. These reservoirs are influenced by sedimentation and diagenesis, which exert a notable effect on their physical properties and pore structure. The delineation of the type of diagenetic phases can be used to select high-quality reservoirs for the study area. Consequently, in the course of subsequent oil and gas exploration and development, it is imperative to further fortify the geological survey and reservoir description efforts, refine reservoir characterization, and identify target areas with exploration potential. Concurrently, the development plan and technical measures should be optimized for the petrogenesis and pore structure characteristics of the reservoirs, so as to improve the oil and gas recovery rate and economic benefits.

## Reference

- [1] Huixiao, Zhao, Y., Shao, X., et al. (2019). Petroleum geological conditions, resource potential and exploration direction in the Mesozoic of Ordos Basin. *Marine Oil and Gas Geology*, 24(02), 14–22.
- [2] Luo, A., Yu, J., Liu, X., et al. (2022). Petroleum exploration practice and main understanding in the Mesozoic of Ordos Basin. *Xinjiang Petroleum Geology*, 43(3), 253–260.
- [3] Yin, S., Wu, Z., Wu, X., et al. (2022). Reservoir enrichment pattern of Jurassic Yan'an Formation in Hongde Block, Longdong Area, Ordos Basin. *Oil and Gas Geology*, 43(5), 1167–1179.
- [4] Zou, C., Zhu, R., Wu, S., et al. (2012). Types, characteristics, mechanisms and prospects of conventional and unconventional oil and gas aggregation: Taking tight oil and tight gas in China as an example. *Journal of Petroleum*, 33(2), 173–187.
- [5] Du, Y. (2017). Diagenesis of Long 8 and Long 9 of the Extension Formation in the central Ordos Basin and its influence on reservoir physical properties. *Groundwater*, 39(04), 196–197+242.
- [6] Jiao, T., Cui, Y., Wang, B., et al. (2021). Sedimentary microphase study of Yan9 oil formation group of Yanan Formation in Shijiawan-Baoziwan area. *Fractured Block Oil and Gas Field*, 28(4), 487–492.
- [7] Sun, Y., Guo, F., Peng, X., et al. (2022). Reservoir characteristics and major constraints of meandering rivers: A case study of Yan 9 in Hu Jian Shan Oilfield, Ordos Basin. *Geoscience*, 36(5), 1403–1413.
- [8] Qiu, X., Sun, H., Zhang, C., et al. (2024). Deposit formation conditions and controlling factors of the Jurassic Yan'an Formation reservoirs in the southwestern Ordos Basin. *Oil and Gas Geology and Recovery*, 1–12.
- [9] Zhao, H., Dang, B., Dang, Y., et al. (2020). Sedimentary evolution of the lower part of the Jurassic Yan'an Formation in the Ansei Zhidan area, Ordos Basin, and its control on hydrocarbons. *Journal of Northwest University (Natural Science Edition)*, 50(3), 490–500.
- [10] Ren, Z., Qi, K., Li, J., et al. (2021). Thermodynamic evolutionary history of the Ordos Basin and its control on hydrocarbon formation and enrichment. *Oil and Gas Geology*, 42(5), 1030–1042.
- [11] Zhao, Y., Qi, Y., Luo, A., et al. (2016). Application of fluid inclusions and authigenic illite dating to reconstruct the hydrocarbon charging history of Jurassic reservoirs in the Ordos Basin. *Journal of Jilin University (Earth Science Edition)*, 46(6), 1637–1648.
- [12] Guo, L., Sun, Y., Guo, F., et al. (2023). Characteristics and main controlling factors of tight sandstone reservoir in delta front facies in Chang 6 member of Yanchang Formation, Hujianshan Oilfield. *Journal of Henan Polytechnic University (Natural Science)*, 42(4), 76–85.
- [13] Chen, C., Fu, L., Chen, X., et al. (2021). Quantitative evaluation method of microscopic inhomogeneity in dense sandstone: A case study of the Chang6 oil formation of the Yanchang Group in the Huaqing area of the Ordos Basin. *Journal of Sedimentology*, 39(05).
- [14] He, D., Ying, F., Zheng, J., et al. (n.d.). Numerical simulation of clastic rock formation and its application. *Numerical Simulation of Clastic Rock Formation and Its Application*.
- [15] Beard, D. C., & Weyl, P. K. (1973). Influence of texture on porosity and permeability of unconsolidated sand. *AAPG Bulletin*, 57(2), 349–369. <https://doi.org/10.1306/819A4272-16C5-11D7-8645000102C1865D>
- [16] Athy, L. F. (1930). Density, porosity, and compaction of sedimentary rocks. *AAPG Bulletin*, 14(1), 1–24. <https://doi.org/10.1306/3D93289E-16B1-11D7-8645000102C1865D>
- [17] Bu, G., Chen, C., Cheng, J., et al. (2019). Analysis of the pre-Jurassic paleomorphology and reservoir formation conditions in the Hujianshan area. *Broken Block Oil and Gas Field*, 26(01), 1–6.

- [18] Fan, T., Zhou, M., Guo, Y., et al. (2024). Pre-Jurassic paleomorphic features and oil and gas formation patterns in the Hujianshan area, Ordos Basin. *Energy and Environmental Protection*, 46(07), 1–7.
- [19] Ge, Y., Dong, L., & Shi, P. (2018). Characteristics and distribution of calcareous cemented sandstones and their influence on reservoirs. *Energy and Environmental Protection*, 40(09), 81–87+93. <https://doi.org/10.1080/15567036.2017.1405113>
- [20] Li, W., Liu, X., Zhang, Q., et al. (2019). Sedimentary evolution of the Middle and Late Triassic extension in the Ordos Basin. *Journal of Northwest University (Natural Science Edition)*, 49(4), 605–621.
- [21] Sun, P. (2016). *Petrophysical modeling and non-homogeneity characterization based on the Donghe sandstone reservoir in Donghe 1 oilfield* [Doctoral dissertation, China University of Petroleum (Beijing)].
- [22] Wang, L., Deng, X., Chu, M., et al. (2022). Formation and distribution of laumontite in sedimentary sequences and their exploration significance: A case study on the Middle–Upper Triassic Yan Chang Formation in Ordos Basin. *Geological Review*, 68(6), 2188–2206.
- [23] Zhang, C., Liu, X., Yang, Y., et al. (2021). History of oil and gas exploration in Changqing Oilfield, Ordos Basin and its revelation. *Xinjiang Petroleum Geology*, 42(3), 253–263.
- [24] Zhou, X., Hui, X., Deng, X., et al. (2019). Distribution pattern of Mesozoic oil reservoirs in Yanchi area, Ordos Basin and the main controlling factors of reservoir formation. *Journal of Northwest University (Natural Science Edition)*, 49(2), 268–279.
- [25] Zhang, G., Liu, W., Han, Y., et al. (2020). Reservoir characterization and factors influencing physical properties of Long 4+5 oil formation group in Fanxue area, Dingbian Oilfield, Ordos Basin. *Northwest Geology*, 53(02), 213–222.

### Copyrights

Copyright for this article is retained by the author(s), with first publication rights granted to the journal.

This is an open-access article distributed under the terms and conditions of the Creative Commons Attribution license (<http://creativecommons.org/licenses/by/4.0/>).